JOURNAL OF SPACECRAFT AND ROCKETS
Vol. 38, No. 5, September–October 2001

Gasdynamics and Heat Transfer Modeling in Rocket Joints

Qunzhen Wang,* Edward C. Mathias,† Joe R. Heman,‡ and Cory W. Smith‡
Thiokol Propulsion, Brigham City, Utah 84302

A new thermal-flow simulation code has been developed to model the gasdynamics and heat transfer, as well as O-ring and flow path erosions inside the space shuttle solid rocket motor joints by combining a thermal analyzer and a general-purpose computational fluid dynamics code. The pressure, temperature, and velocity of the combustion gas in the leak paths are obtained by solving the time-dependent Navier–Stokes equations, whereas the solid temperature is calculated using the heat conduction equation. The gas and solid are coupled by the heat flux at the solid–gas interface. The results of a few test cases are compared with exact solutions or experimental data. These cases include both steady and transient problems involving area change, friction, and heat transfer between gas and solid, as well as mass addition due to the erosion of solid walls. In addition, a set of space shuttle solid rocket motor nozzle joint-4 subscale hot-flow tests is modeled, and the predicted pressures, temperatures (both gas and solid), as well as O-ring erosions are compared with the measured data.

Nomenclature

A	=	cross-sectional area, m^2
A_s	=	surface area, m^2
a	=	width, m
b	=	height, m
C_0, C_1, etc.	=	constant
c_p	=	specific heat at constant pressure, J/kg · K
c_v	=	specific heat at constant volume, J/kg · K
D_h	=	hydraulic diameter, m
E_i	=	inviscid flux term
E_v	=	viscous flux term
e	=	total energy, J/m^3
f	=	Darcy friction factor
H	=	stagnation enthalpy, J/kg
h	=	heat transfer coefficient, W/m^2 · K
K	=	minor loss coefficient
k	=	thermal conductivity, W/m · K
L	=	standoff distance, m
Le	=	Lewis number
m	=	mass, kg
$\dot{m}$	=	mass flow rate, kg/s
$\dot{m}_e$	=	rate of mass addition due to surface erosion, kg/s
Nu	=	Nusselt number, hD/k
Pr	=	Prandtl number, $\mu c_p/k$
p	=	pressure, Pa
Q	=	unknown matrix in the Navier–Stokes equations
q	=	heat transfer rate per unit mass of gas, W/kg
q_1	=	heat flux in the x direction, kg/s^3
$\dot{q}$	=	heat transfer rate, W
R	=	gas constant, J/kg · K
Re	=	Reynolds number, $\rho u D/\mu$
S	=	source term
St	=	Stanton number, $h/\rho u c_p$
T	=	temperature, K
t	=	time, s
u	=	velocity, m/s
V	=	volume, m^3
V_{grad}	=	nondimensional velocity gradient
x	=	distance, m
γ	=	ratio of specific heats
ε	=	roughness, m
μ	=	viscosity, N · s/m^2
ρ	=	density, kg/m^3
τ_{11}	=	stress, Pa

Subscripts

g	=	gas
w	=	wall

Introduction

IT is important to predict accurately the pressure and temperature, as well as the amount of O-ring erosion in the space shuttle reusable solid rocket motor (RSRM) joints in the event of a leak path. The scenarios considered are typically hot combustion gas rapid pressurization events of small volumes through narrow, restricted flow paths. The ideal method for this prediction is a transient three-dimensional computational fluid dynamics (CFD) calculation with computational domain including both the combustion gas and the surrounding solid regions. However, this method has not yet been demonstrated to be economical for this application due to the enormous amount of CPU time and memory required. Consequently, all CFD applications in RSRM joints[1,2] are steady-state simulations with solid regions being excluded from the computational domain by either assuming a constant wall temperature or assuming no heat transfer between the hot combustion gas and cool solid walls.

Currently there are two computer codes, known to the authors, available to model the gas dynamics, heat transfer, and O-ring erosion in the RSRM joint pressurization process. One code is ORING2,[3–6] and the other code is JPR.[7] A way to improve the current prediction technique is to modify the transient compressible flow calculation because the pressure, temperature, and velocity of the combustion gas are not calculated from the time-dependent Navier–Stokes equations in both ORING2 and JPR. Instead, some empirical correlations are used to predict the gas temperature, mass flow rate, and other flow properties by assuming a quasi-steady flow in a constant cross-sectional area pipe, that is, there is no grid in the paths. Furthermore, ORING2 can only handle configurations with two volumes and two paths, whereas it takes significant coding for JPR to do complicated configurations with more than two volumes.

A new thermal-flow simulation code, SFLOW, has been developed to model the gasdynamics and heat transfer, as well as O-ring and flow path erosion inside the space shuttle RSRM joints. The details are discussed in this paper. The SFLOW methodology eliminates some of the approximations inherent in other simulation

Received 30 December 2000; revision received 4 April 2001; accepted for publication 7 April 2001.

*Principal Engineer, M/S 252, Gas Dynamics Section, P.O. Box 707. Member AIAA.
†Principal Engineer, M/S 252, Heat Transfer Section, P.O. Box 707. Member AIAA.
‡Senior Engineer, M/S 252, Heat Transfer Section, P.O. Box 707.

and prediction tools by combining SINDA/G®,[8] a commercial thermal analyzer, and SHARP®,[9–14] a general-purpose CFD code. The pressure, temperature, and velocity of the combustion gas in the leak paths are calculated in SHARP by solving the time-dependent Navier–Stokes equations, whereas the heat conduction in the solid is modeled by SINDA/G. SHARP and SINDA/G are coupled by the heat transfer at the solid–gas interface. The number of flow paths and volumes in SFLOW is limited only by the memory of the computer used to run SFLOW.

Although SHARP can solve one-dimensional, two-dimensional, and three-dimensional flow problems, the flow inside paths is assumed to be one-dimensional in the current version of SFLOW to reduce the CPU time and memory requirements. This approximation is reasonable because leak paths are usually narrow. The solid in SFLOW, however, can be one-dimensional, two-dimensional, and three-dimensional because it is not always a good approximation to assume the heat conduction in the solid region to be one dimensional, especially when the wall material is metal. This treatment is feasible in terms of CPU time and memory because there is only one equation, that is, conservation of energy, to solve in the solid region compared to five equations, that is, conservation of mass, momentum, and energy, needed in the gas region if the flow is modeled as three dimensional. Furthermore, a larger time step can be used in the solid calculation than that used in the gas calculation because the solid temperature usually changes much slower than the flow properties. This way, SFLOW is much more accurate than JPR and ORING2 because the time-dependent gas equations are solved, whereas an SFLOW run takes much less CPU time than a transient three-dimensional CFD calculation because of the one-dimensional flow assumption and the larger time step in the solid region.

The SHARP main program is converted into a subroutine so that it can be called from SINDA/G. The input for this subroutine includes the heat flux from gas to wall, friction factor of the flow path, mass addition due to erosion, gas properties, and grid, as well as boundary and initial conditions, whereas the output is the pressure, temperature, and velocity of the gas for each flow cell at a specific time step. In SFLOW, the flow calculation, that is, SHARP, and the solid calculation, that is SINDA/G, are decoupled from each other such that a smaller time step can be applied in SHARP than that used in SINDA/G. Furthermore, SHARP can use more cells for the flow solution than the number passed from SINDA/G solid surfaces.

As a general-purpose CFD code, SHARP does not have the friction term in the one-dimensional governing equations because it is typically used for two-dimensional and three-dimensional flow simulations where the friction is implicitly taken into account by the viscous force in the resolved near-wall region or by a wall function. In one-dimensional flows, however, the friction term has to be explicitly added because the velocity gradient in the wall-normal direction does not exist. Similarly, a heat transfer term is added to the SHARP equations because the thermal boundary layer is not simulated in SFLOW. Moreover, a mass addition term is added in SHARP because the erosion of the wall material will generate mass. Finally, minor loss terms such as those due to sudden expansion or contraction and flow direction change are accounted for by specifying a loss coefficient in the SFLOW input file at the appropriate flow cells.

The details of the solution scheme, including the modeling of gasdynamics and heat transfer, as well as O-ring and path erosion, are discussed in the next section, followed by comparison of SFLOW predictions to exact solutions or experimental data. The test cases included Fanno flow, where friction is important; Rayleigh flow, where heat transfer between gas and solid is important; flow with mass addition due to the erosion of the solid wall; and transient volume venting process; as well as some transient one-dimensional flows with analytical solutions derived by Cai.[15] In addition, SFLOW has been applied to model the RSRM nozzle joint-4 subscale hot-flow tests,[16] which simulate flows to the primary and secondary O-rings. The predicted pressure, temperature (both gas and solid), and O-ring erosion from SFLOW are compared with the measured data in this paper.

Gasdynamics and Thermal Modeling

Gasdynamics Modeling

In SFLOW, the gas can be either in a flow path or a volume, that is, cavity, which are treated very differently. The gas in a volume is assumed to be in quasi equilibrium with uniform pressure, temperature, and no velocity, whereas that in a path is solved from the first principles, that is, conservation of mass, momentum and energy.

Gas Flow in Paths

The transient compressible flow in a path is modeled using SHARP, which is a density-based general-purpose CFD code. In SHARP, the Navier–Stokes equations are solved on structured grids with multiblock topologies using a finite volume approach (see Refs. 12–14 for details). The gas properties, for example, specific heat at constant pressure, can be functions of temperature. The widely used two-equation k–ε turbulence model is applied to take into account the effect of turbulent fluctuations on the mean motion. The time advancement can be either explicit or implicit for transient flow problems. When the implicit scheme is used, the convergence criterion is that the residual drops by, for example, three orders of magnitude. The grid sensitivity is determined by comparing results from fine and coarse grids.

In one-dimension problems, SHARP solves the Navier–Stokes equations as

$$\frac{\partial Q}{\partial t} + \frac{\partial (E_i - E_v)}{\partial x} = S \tag{1}$$

where the unknowns are

$$Q = A \begin{bmatrix} \rho \\ \rho u \\ e \end{bmatrix} \tag{2}$$

The total energy in Eq. (2) is

$$e = \rho\left(c_v T + \tfrac{1}{2}u^2\right) \tag{3}$$

The inviscid flux term is given by

$$E_i = A \begin{bmatrix} \rho u \\ \rho u^2 + p \\ (e + p)u \end{bmatrix} \tag{4}$$

whereas the viscous term is

$$E_v = A \begin{bmatrix} 0 \\ \tau_{11} \\ u\tau_{11} + q_1 \end{bmatrix} \tag{5}$$

The source term in Eq. (1) is

$$S = \begin{bmatrix} \dot{m} A / V \\ -\dfrac{f A \rho u |u|}{2 D_h} - \dfrac{1}{2}\dfrac{\partial (K A \rho u |u|)}{\partial x} \\ -\dot{q}\dfrac{A}{V} - \dfrac{f A \rho |u|^3}{2 D_h} - \dfrac{1}{2}\dfrac{\partial (K A \rho u^3)}{\partial x} \end{bmatrix} \tag{6}$$

The boundary conditions for the path are obtained from the pressure and temperature of the volumes. A path has to be connected with a volume at one end; the other end can be connected to a volume or a solid wall, which could be either adiabatic or conducting heat away to the solid region.

Note that, similar to other general-purpose CFD codes, SHARP does not have the friction term shown in Eq. (6) because it is typically used for two- and tree-dimensional flow simulations, where the friction is implicitly taken into account by the viscous force in the resolved near-wall region or by the wall function applied. In one-dimensional flows, however, the friction term has to be explicitly accounted for because the velocity gradient $\partial u / \partial y$ does not exist. Similarly, the heat transfer term in Eq. (6) is added to SHARP because the thermal boundary layer is not simulated in SFLOW. The

mass addition terms are also added because the erosion or decomposition of the walls will generate this effect. Finally, minor loss terms such as those due to sudden expansion or contraction and turns or bends in the flow path are added in Eq. (6).

Friction Factor in the Flow Paths

The friction factor in Eq. (6) is obtained from the empirical correlation of Idelchik,[17] which depends on both the shape of the path, that is, circular, rectangular, or triangular, and whether the flow is laminar, turbulent, or in transition. According to Idelchik,[17] the gas flow is divided into laminar, turbulent, and transitional regimes depending on the cutoff Reynolds numbers defined as

$$Re_a = 754\exp(0.0065D_h/\varepsilon) \tag{7}$$

$$Re_b = 1160(D_h/\varepsilon)^{0.11} \tag{8}$$

$$Re_c = 2090(D_h/\varepsilon)^{0.0635} \tag{9}$$

The flow is laminar if the Reynolds number is below Re_a, turbulent if the Reynolds number is above Re_c, and in the transitional regime if the Reynolds number is between Re_a and Re_c. If there are two transitional zones, Re_b is used to determine which of the two zones the flow is in.

The friction factor in the flow path is then determined based on the flow Reynolds number, specifically, for $Re < Re_a$:

$$f = 64/Re \tag{10}$$

For $Re_a \le Re < Re_b$:

$$f = 4.4Re^{-0.595}\exp(-0.00275\varepsilon/D_h) \tag{11}$$

For $Re_b \le Re < Re_c$:

$$f = \left[0.145(\varepsilon/D_h)^{0.244} - I\right]\exp\left[-0.0017^2(Re_c - Re)^2\right] + I \tag{12}$$

where

$$I = 0.758 - 0.0109(\varepsilon/D_h)^{-0.286} \tag{13}$$

For $Re \ge Re_c$:

$$1/\sqrt{f} = -2\log\left[(\varepsilon/3.7D_h) + \left(2.51/Re\sqrt{f}\right)\right] \tag{14}$$

For $Re_a \le Re < Re_c$ and $Re_b \le Re_a$ there is only one transitional zone and

$$f = (7.244Re^{-0.643} - 0.32)\exp\left[-0.0017^2(Re_c - Re)^2\right] + 0.032 \tag{15}$$

Pressure and Temperature in Volumes

Once the flowfield in the path is solved by SHARP, the pressure and temperature in the volumes can be obtained from mass conservation:

$$\frac{\partial}{\partial t}(m) = \dot{m}_e + \sum \dot{m} \tag{16}$$

and energy conservation:

$$\frac{\partial}{\partial t}(mc_v T) = \sum \dot{m}H - \dot{q} \tag{17}$$

where the summation is for all paths that connect to this volume and $\dot{q}$ is the heat transfer rate from the gas to the solid boundary that includes the convective heat transfer as well as the heat transfer due to erosion. In addition to Eqs. (16) and (17), the ideal gas law

$$pV = mRT \tag{18}$$

was used to solve the pressure p, temperature T, and mass m of the volume.

Heat Transfer Modeling

The convective heat transfer between the gas and the solid wall is modeled as

$$\dot{q} = hA_s(T_g - T_w) \tag{19}$$

This heat transfer rate is used in both SHARP and SINDA/G so that the total energy in the system is conserved.

Heat Transfer in Paths

The heat transfer coefficient in flow paths can be obtained from the Nusselt number as

$$h = Nu(k/D_h) \tag{20}$$

The Nusselt number depends on both the cross-sectional shape of the path and the flow regime. If the flow is laminar and the path is circular,

$$Nu = 4.36 \tag{21}$$

whereas for rectangular paths

$$Nu = 1.18135 + 2.30595r^{0.403245} \tag{22}$$

where

$$r = \min\left[16, \frac{\max(a,b)}{\min(a,b)}\right] \tag{23}$$

For turbulent flow, the Nusselt number is calculated using the following empirical correlation:

$$Nu = \frac{f\,Pr\,Re}{\max\left\{Pr^{\frac{2}{3}}, \left[1.07 - 12.7\sqrt{f/8}\left(Pr^{\frac{2}{3}} - 1\right)\right]\right\}}\left(\frac{\mu_g}{\mu_w}\right)^{0.14} \tag{24}$$

In the transitional regime, a linear interpolation between the laminar and turbulent Nusselt number is applied.

Jet Impingement Heat Transfer

The jet impingement heat transfer correlation used in SFLOW is the same as that in ORING2 and JPR, which depends on the standoff distance to diameter ratio, as well as whether the flow is laminar, turbulent, or in the transitional regime. The heat transfer coefficient is obtained from the Stanton number as

$$h = Stc_p(\dot{m}/A) \tag{25}$$

If the flow is laminar, the Stanton number is

$$St = 0.763Pr^{-0.6}\sqrt{1/Re}(T_g/T_w)^{\frac{1}{6}} \tag{26}$$

where the Reynolds number Re is calculated at the jet exit. For turbulent flow with a standoff distance to jet diameter ratio $L/D_h < 2.6$,

$$St = 0.763Pr^{-0.6}\sqrt{V_{\text{grad}}/Re}(T_g/T_w)^{\frac{1}{6}} \tag{27}$$

whereas for $L/D_h > 2.6$

$$St = 0.442Pr^{-0.6}\left(1 + \frac{Le^{0.52} - 1}{2}\right)\sqrt{\frac{2LV_{\text{grad}}}{D_h Re}}\left(\frac{T_g}{T_w}\right)^{\frac{1}{3}} \tag{28}$$

The velocity gradient in the preceding equations is

$$V_{\text{grad}} = 1 \tag{29}$$

for $L/D_h < 3.4$,

$$V_{\text{grad}} = 1 - 0.196\left[(L/D_h - 3.4)/5\right]^2 \tag{30}$$

for $3.4 < L/D_h < 8.4$, and

$$V_{\text{grad}} = \frac{1 - \exp[-1/(0.2315L/D_h - 0.74)]}{0.13L/D_h - 0.39} \tag{31}$$

for $L/D_h > 8.4$. If the flow is in transitional regime, the heat transfer coefficient is obtained by linear interpolation between laminar and turbulent regimes.

Heat Transfer in Volumes

The heat transfer from the gas in a volume to the solid boundary can be modeled in four different ways: 1) using the impingement jet heat transfer correlation described earlier, 2) using the heat transfer coefficient in the paths connected to this volume, 3) using a conduction length as $h = k/l$, and 4) using a user-specified heat transfer coefficient. The user of SFLOW specifies which of these methods should be applied to calculate heat transfer coefficient for all of the gas–solid interfaces in all volumes.

Erosion Modeling

The erosion model used in SFLOW is the same as that in ORING2 and JPR. Specifically, the erosion rate is a function of heat transfer coefficient between gas and solid and the gas temperature, as well as the wall temperature. Erosion has the following effects on the gas: 1) it increases the cross-sectional area of the path or the volume of the cavity, 2) it adds mass to the gas, and 3) it adds energy to the gas.

Validation Cases

For all validation cases shown in this section, there are only two volumes connected by one flow path. The pressure and temperature in one or both volumes are specified as input, whereas the pressure, temperature, and velocity in the flow path are calculated using SFLOW. Most of these tests are for SHARP in solving one-dimensional flow problems with friction, heat transfer, mass addition, and area change because no modification is made to the commercial thermal code SINDA/G.

Fanno Flow

For air entering an adiabatic 30.48-m-diam duct with a total pressure of 0.1524 MPa and total temperature of 300 K, it can be shown analytically that the inlet and outlet Mach number will be 0.8 and 0.9, respectively, if the friction coefficient is assumed to be 0.0578, the pipe length is 30.48 m, and the outlet pressure is 0.08758 MPa. SFLOW was used to simulate this test case, and the results are compared with the analytical solutions in Table 1. It is clear that the error in the predicted Mach number is smaller when more flow cells are applied. However, the error drops much more from 20 cells to 200 cells than that from 200 cells to 1000 cells. For this particular case, 200 cells are enough to keep the error in both inlet and outlet Mach number below 0.55%.

Rayleigh Flow

For air entering a frictionless 0.03048-m-diam, 30.48-m-long duct with a total pressure of 0.0709 MPa and total temperature of 291.1 K, it can be shown analytically that the inlet and outlet Mach number will be 0.2 and 0.25, respectively, if the heat addition is assumed to be 140.4 kJ/kg, and the outlet pressure is 0.0665 MPa. SFLOW was used to simulate this test case, and the results are shown in Table 2. For this particular case, 200 cells are enough to keep the error in both inlet and outlet Mach number below 0.65%.

Table 1 Predicted Mach number for the Fanno flow test case

Mach	20 cells	200 cells	1000 cells
M_{in}	0.8232	0.8043	0.8027
Error in M_{in}, %	2.90	0.54	0.34
M_{out}	0.8900	0.8954	0.8958
Error in M_{out}, %	1.11	0.51	0.47

Table 2 Predicted Mach number for the Rayleigh flow test case

Mach	20 cells	200 cells	1000 cells
M_{in}	0.1954	0.1987	0.1991
Error in M_{in}, %	2.30	0.65	0.45
M_{out}	0.2498	0.2484	0.2485
Error in M_{out}, %	0.08	0.64	0.60

Table 3 Predicted Mach number for the mass addition test case

Mach	20 cells	200 cells	1000 cells
M_{in}	0.5039	0.5019	0.5018
Error in M_{in}, %	0.78	0.38	0.36
M_{out}	0.5898	0.5962	0.5967
Error in M_{out}, %	1.70	0.63	0.55

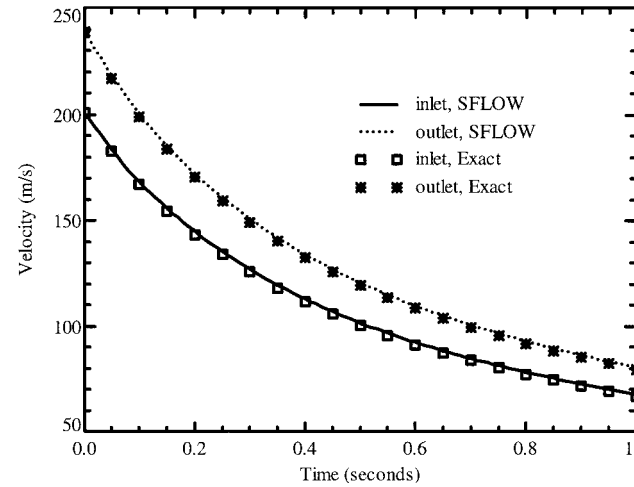

Fig. 1 Comparison of predicted velocity with analytical solution of Eq. (33) for the case of transient flow with area change.

Mass Addition

For air entering a frictionless adiabatic 0.03048-m-diam duct with a total pressure of 0.08178 MPa and total temperature of 291.7 K, it can be shown analytically that the inlet and outlet Mach number will be 0.5 and 0.6, respectively, if 0.009525 kg/s of air at a temperature of 291.7 K is added to the flow and the outlet pressure is 0.068 MPa. SFLOW was used to simulate this test case, and the results are shown in Table 3. With 200 or more flow cells, the error in the inlet Mach number is less than 0.38%, whereas that in the outlet Mach number is less than 0.63%.

Transient Flow with Area Change

All of the test cases shown thus far are steady-state problems so only the SFLOW predictions at long times were compared with the exact steady-state solution. In this and the following three sections, SFLOW was tested using one-dimensional unsteady flow cases with analytical solutions derived by Cai.[15]

For one-dimensional compressible flow in a circular pipe with a cross-sectional area

$$A = C_3/(C_0 x + C_2) \tag{32}$$

the exact solution is

$$p = \text{const}, \qquad \rho = \text{const}, \qquad u = \frac{2C_0(C_0 x + C_2)}{2C_0^2 t + C_1} \tag{33}$$

if both friction and heat transfer are neglected. This transient flow with area change case is simulated using SFLOW with a uniform grid of 20 flow cells by assuming $C_0 = C_1 = C_3 = 1$ and $C_2 = 100$. The flow path is from $x = 0$ to $x = 20$ m and the time is from $t = 0$ to $t = 1$ s. The velocity at the inlet and outlet from SFLOW is compared with the exact solution in Fig. 1, which shows a very good agreement even though only 20 flow cells are used.

Transient Flow with Heat Transfer

For one-dimensional flow in a circular pipe with a heat transfer rate per unit mass of

$$q = \frac{\gamma}{\gamma - 1}\frac{C_1 p}{C_5}\left(\frac{C_1 x + C_3}{C_1 t + C_2}\right)^{1 + C_4/C_1} \tag{34}$$

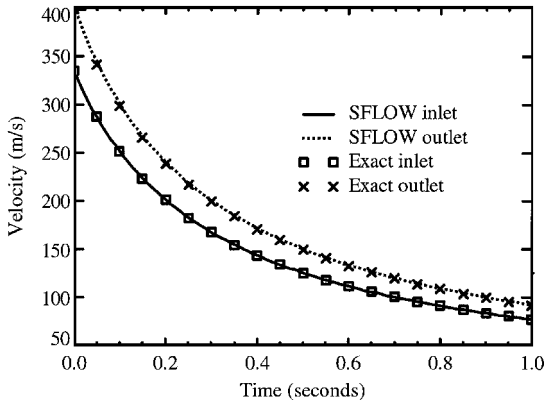

Fig. 2 Comparison of predicted velocity with analytical solution of Eq. (35) for the case of transient flow with heat transfer.

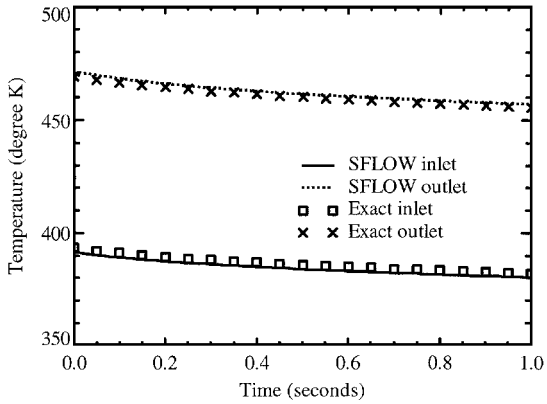

Fig. 3 Comparison of predicted temperature with analytical solution of Eq. (35) for the case of transient flow with heat transfer.

the exact solution is

$$p = \text{const}, \qquad \rho = \frac{C_5(C_1t + C_2)^{C_4/C_1}}{(C_1x + C_3)^{1+C_4/C_1}}, \qquad u = \frac{C_1x + C_3}{C_1t + C_2} \tag{35}$$

if the cross-sectional area is constant and the friction is neglected. This transient flow with heat transfer case was simulated using SFLOW with a uniform grid of 200 flow cells by assuming $C_1 = C_4 = 1$, $C_3 = C_5 = 5000$, and $C_2 = 15$. The flow path is from $x = 0$ to 20 m and the time is from $t = 0$ to 1 s. The velocity and temperature at the inlet and outlet from SFLOW are compared with the exact solution in Figs. 2 and 3. The velocity profile at both the inlet and outlet agree very well with the analytical solution, and the agreement for the temperature is also reasonable. Although not shown here, the results using 20 cells are much worse than those shown in Figs. 2 and 3, and it is expected that a better temperature prediction would be obtained by using even more flow cells.

Transient Flow with Friction and Heat Transfer

For one-dimensional flow in a circular pipe with a heat transfer rate of

$$q = -(16A/\pi f^2 t^3) \tag{36}$$

the exact solution is

$$p = \text{const}, \qquad \rho = \text{const}, \qquad u = 4\sqrt{A}\Big/\sqrt{\pi} ft \tag{37}$$

if both the cross-sectional area and friction factor are constant. This transient flow with heat transfer and constant friction factor case was simulated using SFLOW with a uniform grid of 20 flow cells and $f = 0.004/\sqrt{\pi}$. The flow path is from $x = 0$ to 20 m and the time is from $t = 5$ to 10 s. The velocity at the inlet and outlet, which is the same at any given time according to Eq. (37), from SFLOW is compared with the exact solution in Fig. 4, which shows a very good agreement.

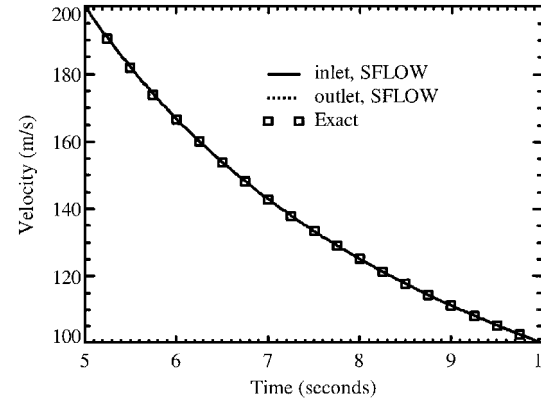

Fig. 4 Comparison of predicted velocity with analytical solution of Eq. (37) for the case of transient flow with friction and heat transfer.

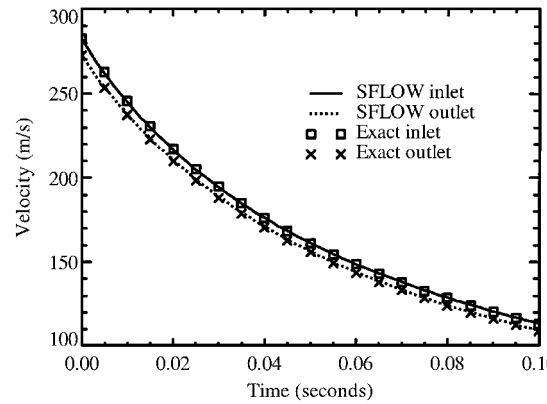

Fig. 5 Comparison of predicted velocity with analytical solution of Eq. (41) for the case of transient flow with area change, friction, and heat transfer.

Transient Flow with Area Change, Friction, and Heat Transfer

For one-dimensional flow in a pipe with area A, friction factor f, and heat transfer rate q given by

$$A = \frac{1}{\left[C_4 \exp(-\sqrt{\pi/C_1}x) + \sqrt{C_x/\pi}\right]} \tag{38}$$

$$f = \frac{4}{\sqrt{C_1\left[C_4 \exp(-\sqrt{\pi/C_1}x) + \sqrt{C_x/\pi}\right]}} \tag{39}$$

$$q = -\sqrt{\frac{\pi}{C_1}}\left\{\frac{C_2[C_4 \exp(-\sqrt{\pi/C_1}x) + \sqrt{C_x/\pi}]}{C_2t + C_3}\right\} \tag{40}$$

the exact solution is

$$p = \text{const}, \qquad \rho = \text{const}$$

$$u = \frac{C_2\left[C_4 \exp\left(-\sqrt{\pi/C_1}x\right) + \sqrt{C_x/\pi}\right]}{C_2t + C_3} \tag{41}$$

This transient flow with area change, friction, and heat transfer case is simulated using SFLOW with a uniform grid of 20 flow cells by assuming $C_0 = C_3 = C_4 = 1$, $C_1 = 1000$, and $C_2 = 15$. The flow path is from $x = 0$ to $x = 20$ m and the time is from $t = 0$ to 0.1 s. The velocity at the inlet and outlet from SFLOW is compared with the exact solution in Fig. 5, which shows a very good agreement even though only 20 flow cells are used.

Volume Venting

The preceding cases focus on the gas flow in paths because only pressure, temperature, and velocity of the gas in the pipe were compared with the analytical solutions. To validate the volume pressure

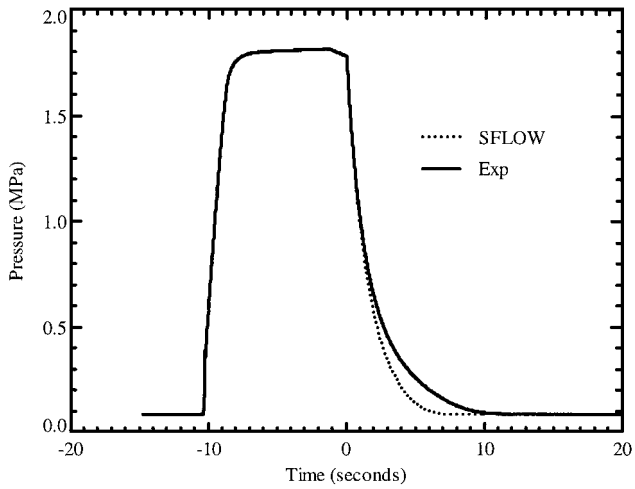

Fig. 6 Comparison of predicted pressure with the experimental data for the volume-venting case; friction and heat transfer neglected in the prediction.

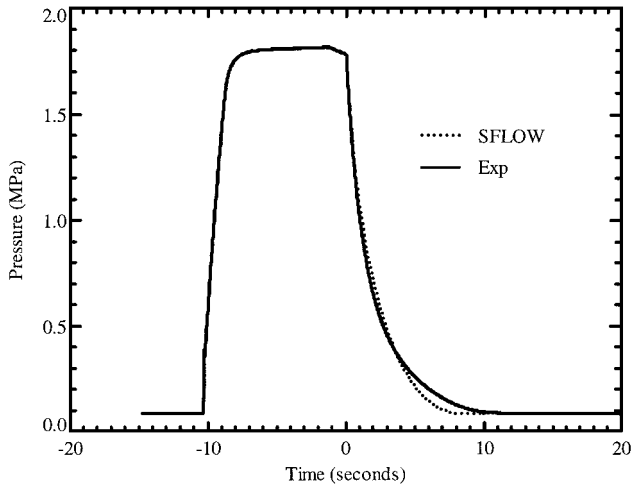

Fig. 7 Comparison of predicted pressure with the experimental data for the volume-venting case; friction and heat transfer accounted for in the prediction.

and temperature algorithm, the SFLOW prediction in a volume-venting experiment is compared with the measured data. In the experiment, a tank with a volume of 9.836×10^{-4} m^3 is connected to a 0.058-m circular pipe with a diameter of 1.829 mm, which is open to ambient conditions at 0.08618 MPa. The tank is at ambient condition initially, and the tank pressure is increased to about 1.779 MPa at $t = 0$ with the valve between the tank and pipe closed. This valve is opened at $t = 0$, and the tank pressure begins to fall. The SFLOW prediction starts from $t = 0$ using 20 flow cells in the pipe. The comparison of the predicted pressure with the experimental data is shown in Fig. 6, which indicates that the predicted pressure is smaller than the measured data.

The friction in the pipe and heat transfer between the gas and solid walls were neglected in the SFLOW results shown in Fig. 6. Figure 7 shows the results with both friction and heat transfer effects being taken into account, which indicates a better agreement with experimental data. This volume-venting case has also been simulated using ISENTANK,[18] which assumes the flow in the path is isentropic. The SFLOW prediction in Fig. 6 is very similar to the result from ISENTANK with a discharge coefficient of 1.0, whereas that in Fig. 7 is similar to that from ISENTANK with a discharge coefficient of 0.6.

RSRM Nozzle Joint-4 Test

SFLOW was also used to simulate the RSRM nozzle joint-4 hot fire test,[16] which was also modeled by Clayton.[19] Figure 8 shows the location of joint 4 in the RSRM nozzle and the hot flow test

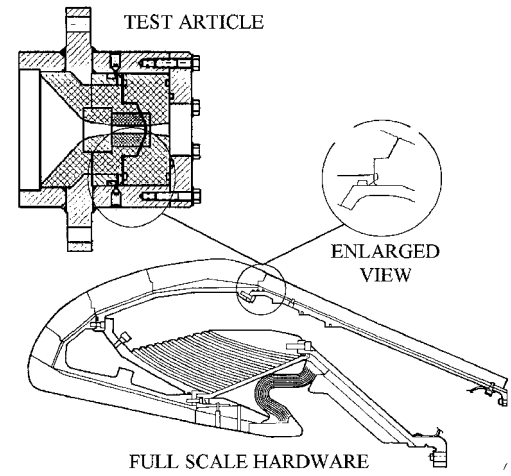

Fig. 8 RSRM nozzle joint-4 and hot-flow test fixture.

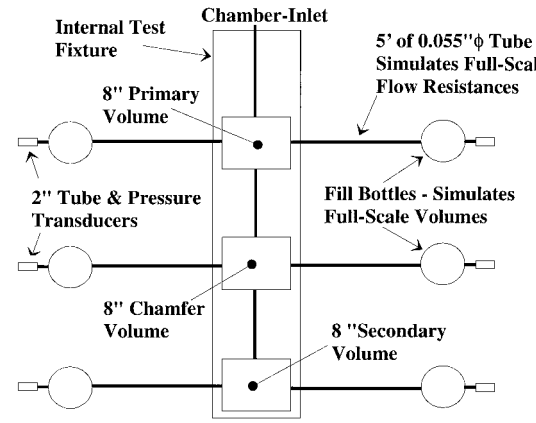

Fig. 9 Schematic of the test fixture for the RSRM nozzle joint-4 hot-flow test.

fixture. The insert is the enlarged view of joint 4. In this section, only comparisons of the SFLOW predictions with the measured data for configuration 8 at the 90-deg side will be discussed. The SFLOW results for other configurations, more results for this configuration, as well as more details of the model will be published later.

A schematic of the test fixture for the RSRM nozzle joint-4 hot-flow test is shown in Fig. 9. There are two fill tubes and bottles connected to the primary O-ring gland and chamfer region, as well as the secondary O-ring gland. The SFLOW model consists of four volumes (the combustion chamber, primary O-ring gland, chamfer region, and secondary O-ring gland) and nine paths (one from the combustion chamber to the primary O-ring gland, one from the primary O-ring gland to the chamfer region, one from the chamfer region to the secondary O-ring gland, two for the fill tubes and bottles connected to the primary O-ring, two for the fill tubes and bottles connected to the chamfer, and two for the fill tubes and bottles connected to the secondary O-ring).

Figure 10 shows the solid grid used for the RSRM nozzle joint-4 simulation. The widths of the leak paths are as follows: 1.702 mm at the chamber and 2.032 mm at the end of leg 1, 1.118 mm for the second leg (horizontal one), 1.168 mm for the third leg (leading to the primary O-ring), 0.508 mm from primary O-ring to chamfer, and 0.127 mm from chamfer to secondary O-ring. The volumes for the primary O-ring cavity, chamfer cavity, secondary O-ring cavity, fill bottles connected to the primary O-ring, chamfer cavity, and secondary O-ring are 1.565×10^{-6}, 4.579×10^{-6}, 5.213×10^{-6}, 1.833×10^{-5}, 1.211×10^{-5}, and 1.46×10^{-5} m^3, respectively. The pressure and temperature in the combustion chamber is specified as input for the SFLOW prediction. (The temperature is 294 K initially and increases to 2777 K at 0.07 s and then remains at that high temperature, and the input pressure is shown later.) Impingement heat transfer is applied for several surfaces on the O-rings, the inlet path, and the chamfer region, while minor losses are applied in the

paths where the flow turns. Steady-state gas-only CFD simulations such as those discussed by Laubacher et al.[1] are used to determine which surfaces should have jet impingement heat transfer.

Isocontours of the predicted temperatures of the solid at 4 s are shown in Fig. 11. Initially the temperature is at 294 K. At 4 s, the solid cells near the impinging surfaces as well as those near the flow path from the chamber to the primary O-ring are hot, while the temperatures at the solid cells farther away are still low. Because the thermal conductivity is larger for steel than carbon cloth phenolic (CCP), a larger region of the steel is at a higher temperature than CCP.

Isocontours of the predicted solid temperatures at different times are shown in Figs. 12–15 for part of the domain including the O-rings and chamfer. At earlier times, the solid temperature near the gas–solid interface increases with time because of the convective heat transfer from the hot combustion gas. At later times, however, more solid heats up, and the solid temperatures near the jet impingement surfaces decreases due to heat conduction. Specifically, the maximum solid temperatures are 294, 2408, 2433, 2287, and 1782 K at 0, 1, 2, 3, and 4 s, respectively.

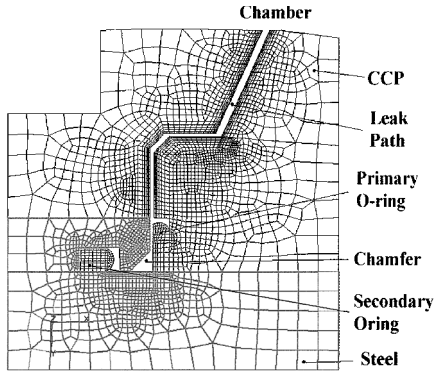

Fig. 10 Solid grid for RSRM joint-4 hot-flow simulations.

Figures 16–18 show the comparison of the SFLOW predicted gas pressure with the experimental data at the fill bottles off the primary O-ring groove, chamfer region, and the secondary O-ring groove in RSRM nozzle joint-4 test. Also shown in Figs. 16–18 is the pressure of the combustion chamber, which is an input to the SFLOW code. The pressures at all of the fill bottles are very similar, and the predicted values agree very well with the measured data.

The predicted gas temperatures of the fill bottles are compared with the measured data in Fig. 19. The agreement is reasonable considering that the chamber temperature is about 2777 K, whereas that in the fill bottles is less than 320 K.

Figures 20 and 21 show the predicted solid temperatures at two locations, one near the primary O-ring (T14 in Fig. 22) and the other just before the secondary O-ring (T15 in Fig. 22), together with the measured data at the same locations. The agreement is reasonable considering that, as discussed by Clayton,[19] the measured solid temperatures are not very accurate due to the large gradients, tiny gaps, and brief timescales. The predicted erosion of the secondary O-ring is shown in Fig. 23. The total erosion after 2 s is about 0.2108 mm, which is very close to the measured value of 0.2032 mm.

As discussed already, most CFD applications in the RSRM joints do not include the solid region in the computational domain, and the solid wall is assumed to be either adiabatic or isothermal. Figures 24 and 25 compare the SFLOW predictions of the pressures and gas temperatures in the fill bottles with and without heat transfer between the gas and solid. The comparison indicates that, without heat transfer, the fill time is reduced by a factor of about three and the

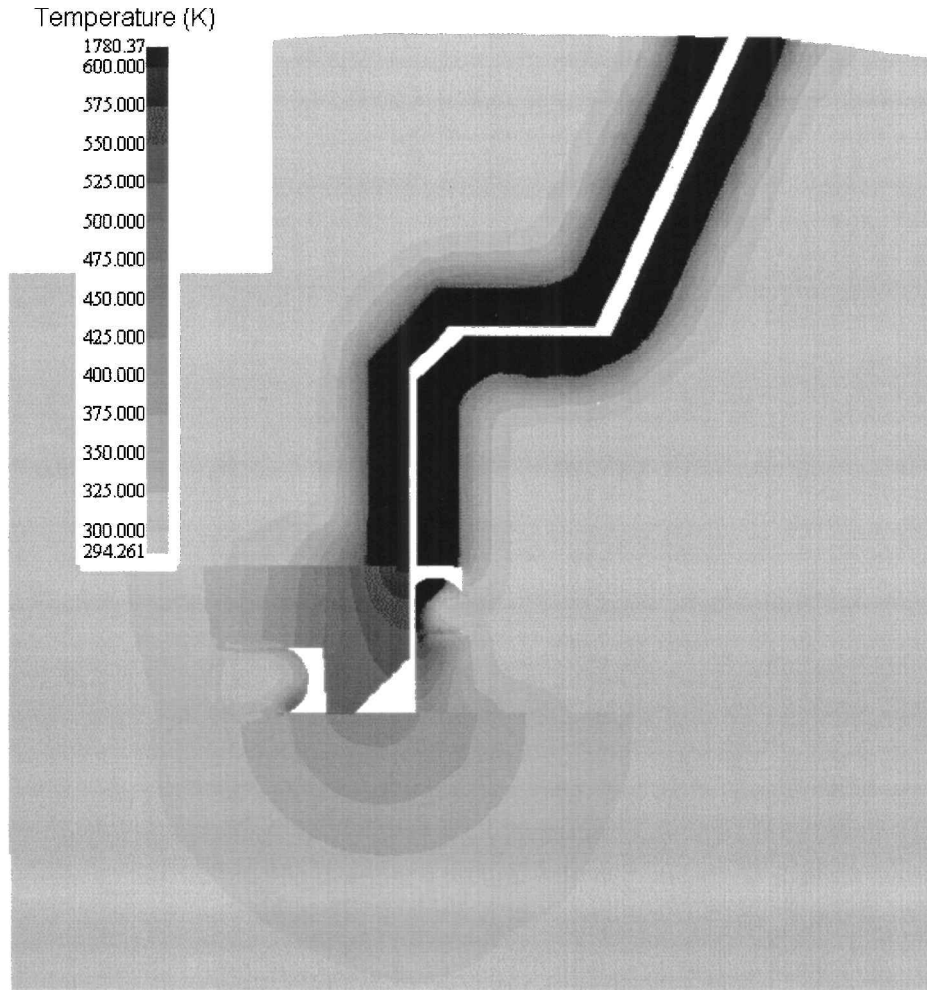

Fig. 11 Isocontours of predicted solid temperature in the whole computational domain at 4 s.

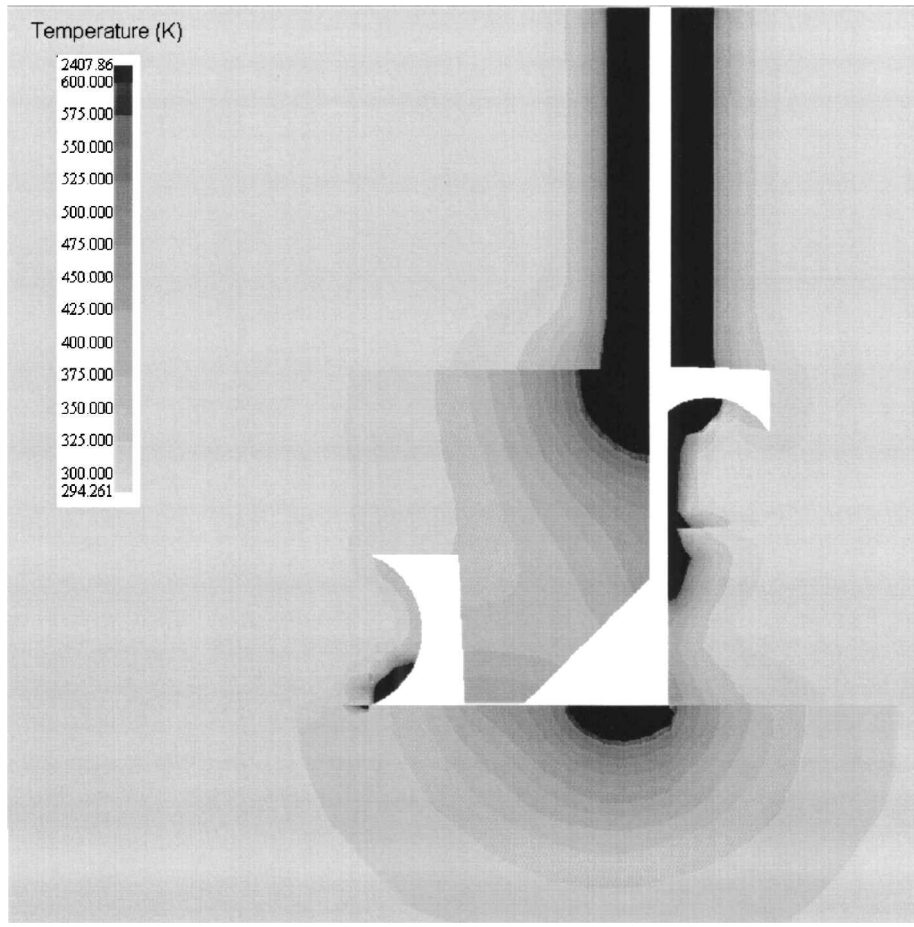

Fig. 12 Isocontours of predicted solid temperature in part of the computational domain at 1 s.

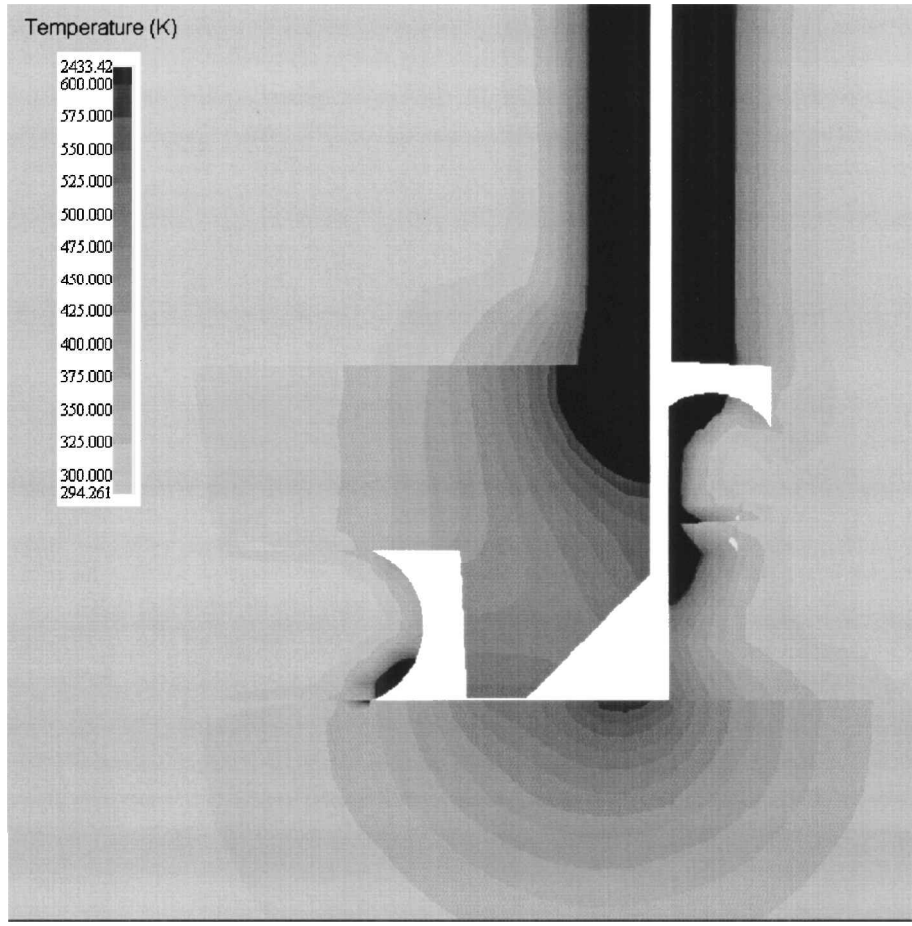

Fig. 13 Isocontours of predicted solid temperature in part of the computational domain at 2 s.

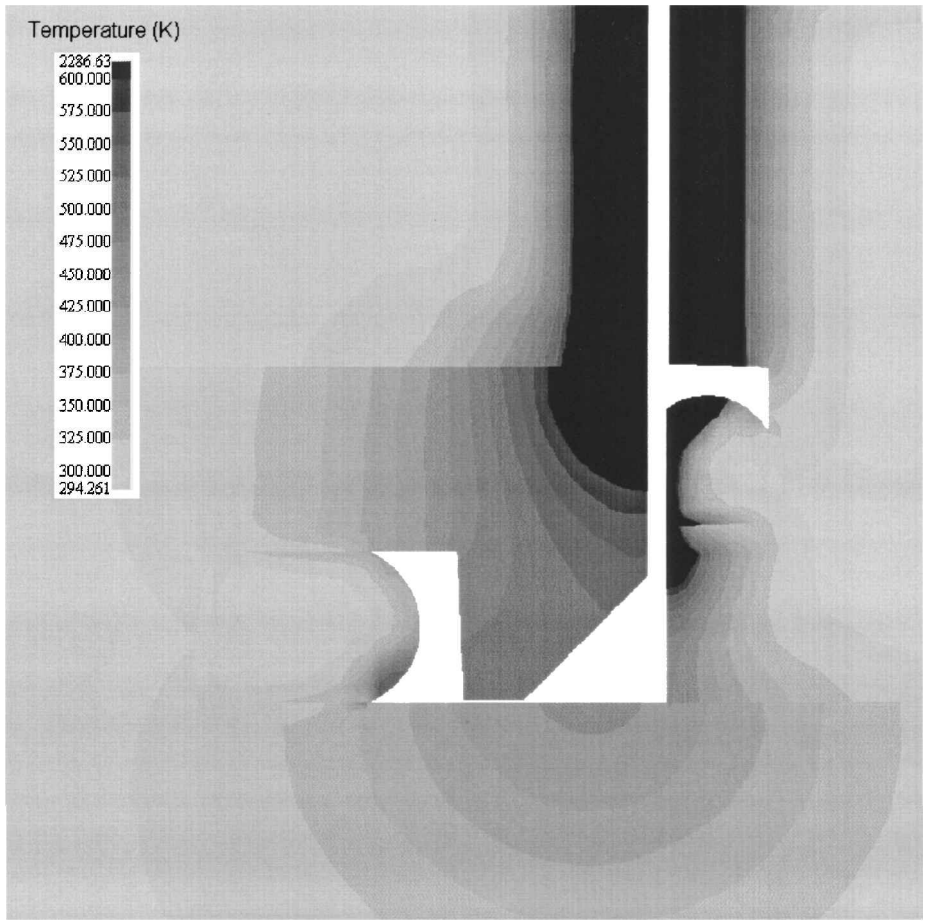

Fig. 14 Isocontours of predicted solid temperature in part of the computational domain at 3 s.

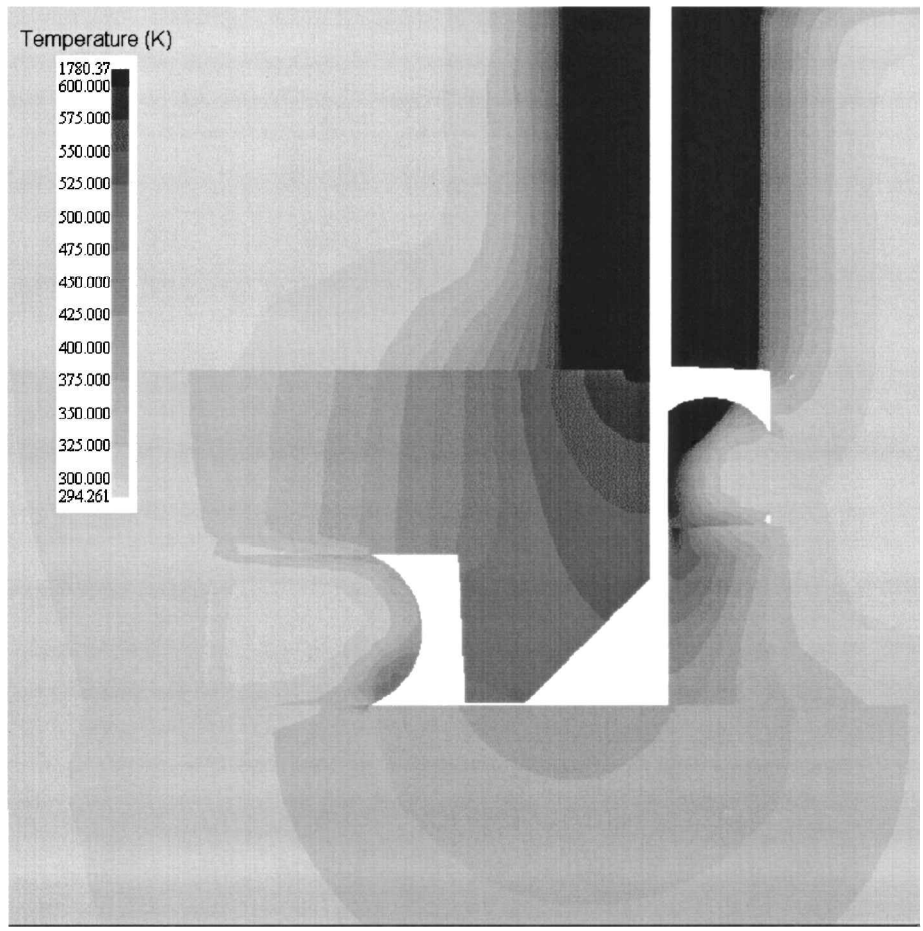

Fig. 15 Isocontours of predicted solid temperature in part of the computational domain at 4 s.

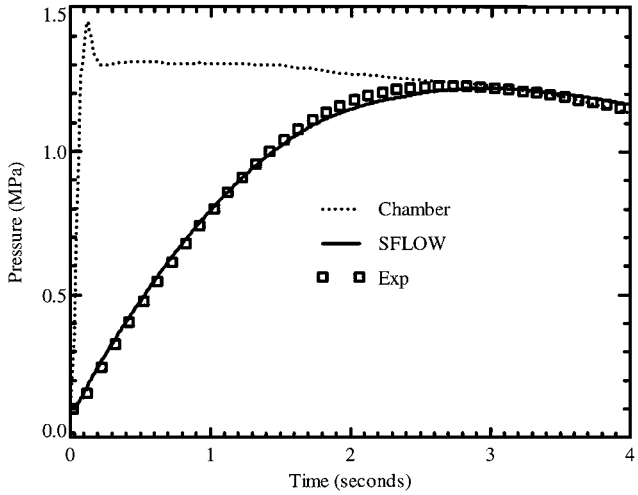

Fig. 16 Comparison of predicted pressure of the fill bottle off primary O-ring grove in RSRM nozzle joint 4 with measured data.

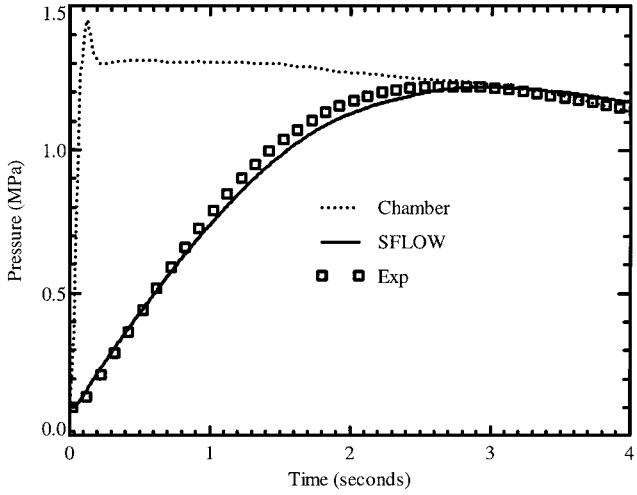

Fig. 17 Comparison of predicted pressure of the fill bottle off chamfer region in RSRM nozzle joint 4 with measured data.

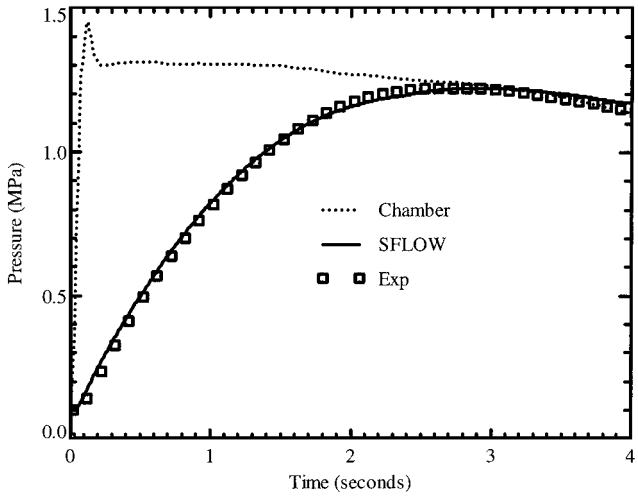

Fig. 18 Comparison of predicted pressure of the fill bottle off secondary O-ring grove in RSRM nozzle joint 4 with measured data.

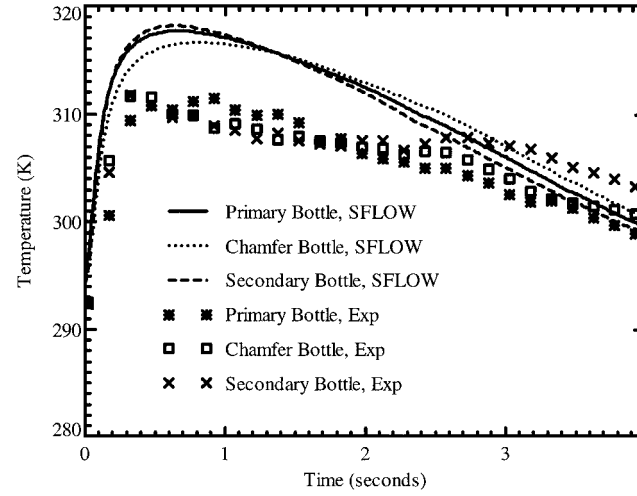

Fig. 19 Comparison of predicted gas temperature of the fill bottles in RSRM nozzle joint 4 with measured data.

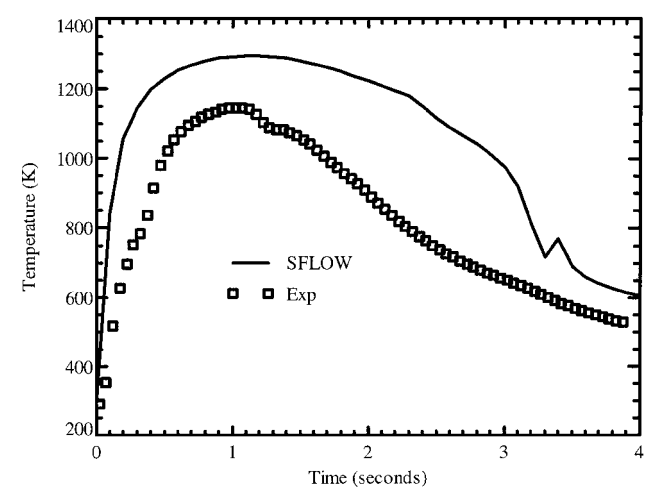

Fig. 20 Comparison of predicted solid temperature near the primary O-ring (T14 in Fig. 22) with measured data.

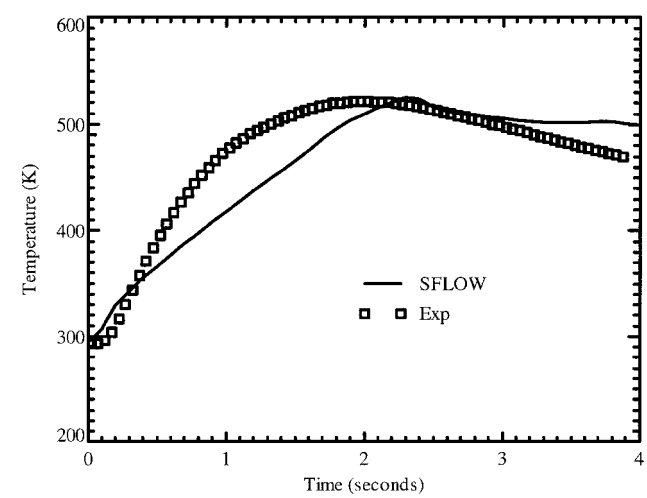

Fig. 21 Comparison of predicted solid temperature near the secondary O-ring (T15 in Fig. 22) with measured data.

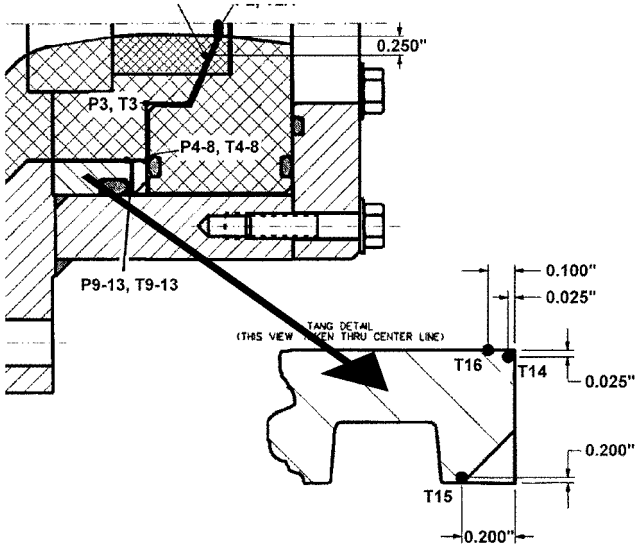

Fig. 22 Locations of thermocouples in the RSRM nozzle joint-4 test.

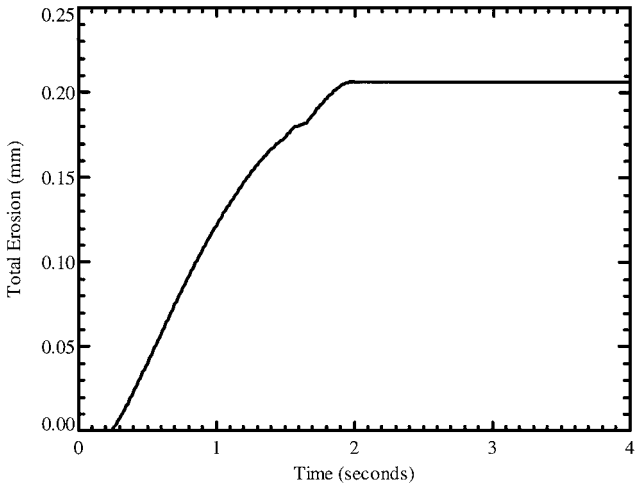

Fig. 23 Predicted secondary O-ring erosion in RSRM nozzle joint 4.

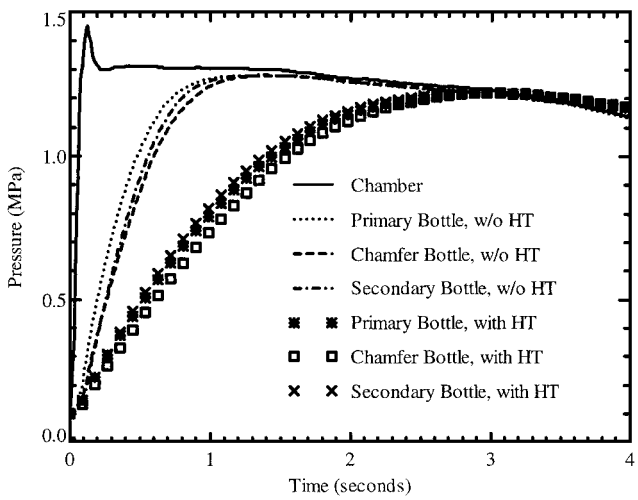

Fig. 24 Comparison of predicted gas pressure at the fill bottles in RSRM nozzle joint 4 with and without the heat transfer between gas and solid.

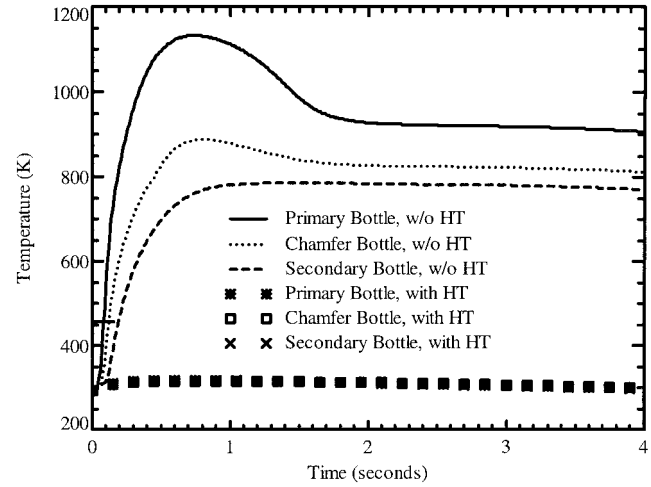

Fig. 25 Comparison of predicted gas temperature at the fill bottles in RSRM nozzle joint 4 with and without the heat transfer between gas and solid.

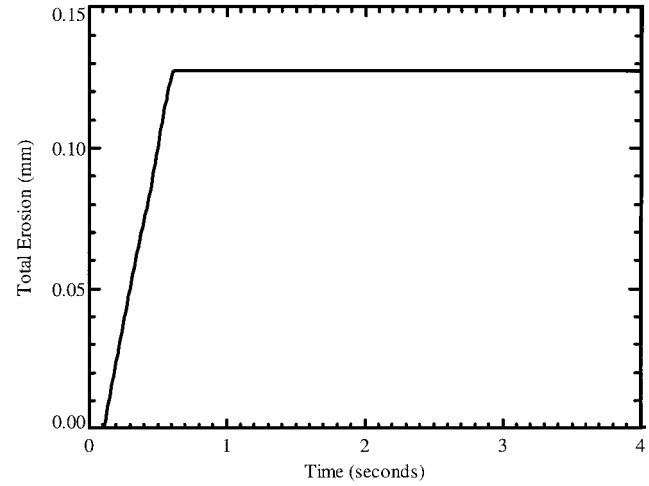

Fig. 26 Secondary O-ring erosion in RSRM nozzle joint 4 from the adiabatic prediction.

gas temperature increases to more than 750 K from around 310 K with heat transfer. For these conditions, heat transfer to the solid wall is a significant driver for the problem. Figure 26 shows that the predicted total erosion for the adiabatic case is 0.127 mm, which is smaller than that shown in Fig. 23 for the case with heat transfer. For the adiabatic case, the erosion rate is larger at earlier times because of the high gas temperature, but the erosion stops earlier (0.6 s instead of 2.0 s) due to the shorter fill time.

Conclusions

A new thermal-flow simulation code, called SFLOW, has been developed to model the gas dynamics and heat transfer, as well as O-ring and flow path erosion inside the space shuttle solid rocket motor joints by combining SINDA/G, a commercial thermal analyzer, and SHARP, a general-purpose CFD code. SHARP was modified so that friction, heat transfer, mass addition, and minor losses in one-dimensional flow can be taken into account. The pressure, temperature, and velocity of the combustion gas in the leak paths are calculated in SHARP by solving the time-dependent Navier–Stokes equations, whereas the heat conduction in the solid is modeled by SINDA/G. The two codes are coupled by the heat flux at the solid–gas interface.

A few test cases are presented, and the results from SFLOW agree very well with the exact solutions or experimental data. These cases include Fanno flow, where friction is important, Rayleigh flow, where heat transfer between gas and solid is important, flow with mass addition due to the erosion of the solid wall, and a transient volume-venting process, as well as some transient one-dimensional flows with analytical solutions. In addition, SFLOW is applied to model the space shuttle solid rocket motor nozzle joint-4 subscale hot-flow tests, and the predicted pressures, temperatures (both gas and solid), and O-ring erosions agree well with the experimental data. It was also found that the heat transfer between gas and solid has a major effect on the pressures and temperatures of the fill bottles as well as O-ring erosion in the RSRM nozzle joint-4 configuration 8 test.

References

[1]Laubacher, B. A., Eaton, A. M., Pate, R. A., Wang, Q., Mathias, E. C., and Shipley, J. L., "Cold-Flow Simulation and CFD Modeling of the Space Shuttle Solid Rocket Motor Nozzle Joints," AIAA Paper 99-2793, July 1999.

[2]Eaton, A., and Mathias, E., "Simulating Heat Transfer to a Solid Rocket Motor Nozzle-Case-Joint Thermal Barrier," AIAA Paper 2000-3807, July 2000.

[3]O'Malley, M. J., "A Model for Predicting RSRM Joint Volume Pressurization, Temperature Transients, and Ablation," AIAA Paper 88-3332, July 1988.

[4]O'Malley, M. J., "ORING2: Volume Filling and O-Ring Erosion Prediction Code with Improved Model Descriptions and Validation, Part I: Improved O-Ring Erosion Prediction Code," Thiokol Corp., Rept. TWR-17030, Brigham City, UT, Aug. 1987.

[5]O'Malley, M. J., "ORING2: Volume Filling and O-Ring Erosion Prediction Code with Improved Model Descriptions and Validation, Part II: Improved Volume Filling Model and Code Validation," Thiokol Corp., Rept. TWR-17031, Brigham City, UT, Nov. 1987.

[6]O'Malley, M. J., "ORING2: Volume Filling and O-Ring Erosion Prediction Code with Improved Model Descriptions and Validation, Part III: User's Guide," Thiokol Corp., Rept. TWR-50398, Brigham City, UT, Feb. 1990.

[7]Clayton, J. L., "Joint Pressurization Routine (JPR) Theoretical Development and Users Manual," NASA Marshall Space Flight Center, MSFC Internal Memorandum ED66 (95-01), Huntsville, AL, Jan. 1995.

[8]"SINDA/G® User's Guide," Network Analysis, Inc., Tempe, AZ, 1996.

[9]Golafshani, M., and Loh, H. T., "Computation of Two-Phase Viscous Flow in Solid Rocket Motors Using a Flux-Split Eulerian–Lagrangian Technique," AIAA Paper 89-2785, July 1989.

[10]Loh, H. T., and Golafshani, M., "Computation of Viscous Chemically Reacting Flows in Hybrid Rocket Motors Using an Upwind LU-SSOR Scheme," AIAA Paper 90-1570, June 1990.

[11]Loh, H. T., Smith-Kent, R., Perkins, F., and Chwalowski, P., "Evaluation of Aft Skirt Length Effects on Rocket Motor Base Heat Using Computational Fluid Dynamics," AIAA Paper 96-2645, July 1996.

[12]Wang, Q., "Theory Manual for SHARP®: a General CFD Solver," Thiokol Corp., Rept. TR-11580, Brigham City, UT, Jan. 1999.

[13]Wang, Q., "Programer's Guide for SHARP®: a General CFD Solver," Thiokol Corp., Rept. TR-11581, Brigham City, UT, Jan. 1999.

[14]Wang, Q., "User's Guide for SHARP®: a General CFD Solver," Thiokol Corp., Rept. TR-11582, Brigham City, UT, Jan. 1999.

[15]Cai, R., "Some Explicit Analytical Solutions of Unsteady Compressible Flow," *Journal of Fluids Engineering*, Vol. 120, Dec. 1998, pp. 760–764.

[16]Prince, A., "Final Report for ETP-1385: Tortuous Path Thermal Analysis Test Bed," Thiokol Corp., Rept. TR-66623, Brigham City, UT, 1999.

[17]Idelchik, I. E., *Handbook of Hydraulic Resistance*, 2nd ed., Hemisphere, New York, 1986, pp. 59–64.

[18]Wang, Q., "ISENTANK Code," Thiokol Corp., Memo 32B2-FY98-M029, Brigham City, UT, June 1998.

[19]Clayton, J. L., "Reusable Solid Rocket Motor Nozzle Joint-4 Test Correlated Gas Dynamics-Thermal Analysis," AIAA Paper 99-2791, July 1999.

I. E. Vas
Associate Editor